Coastal Engineering 193 (2024) 104598

Contents lists available at ScienceDirect

Coastal Engineering

journal homepage: www.elsevier.com/locate/coastaleng

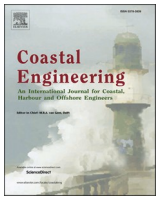

Experimental study on local scour for large-diameter mono-column composite bucket foundation for offshore wind turbines

Yuhang Zhang [a], Jinfeng Zhang [b,*], Zhengqi Li [a], Tongqing Chen [a], Qinghe Zhang [a], Jiandong Xiao [b]

[a] State Key Laboratory of Hydraulic Engineering Intelligent Construction and Operation, Tianjin University, Tianjin, 300072, China
[b] Shanghai Investigation, Design & Research Institute Co., Ltd., Shanghai, 200355, China

ARTICLE INFO

Keywords:
Mono-column composite bucket
Local scour
Equilibrium scour topography
Scour depth prediction

ABSTRACT

The issue of seabed scour around offshore wind turbine foundations is a significant safety concern. In this study, local scour around a specific type of foundation, known as the large-diameter Mono-Column Composite Bucket Foundation (MCCBF) with six connectors, has been investigated through physical experiments. The study involved various flow conditions, including unidirectional flows, tidal flows, and combinations of regular waves and currents. It has been found that under similar flow intensity and orientation angles, unidirectional flow tends to cause deeper scour depths, but with a more limited extent compared to scour induced by tidal flows. The disparity in maximum scour depth between tidal and unidirectional flows decreases as flow velocity increases. Under regular wave-current interaction, both the scour depth and the scour extent are larger than those induced by unidirectional flow. The presence of lee-wake vortices and streamline contractions near the connectors results in larger scour depths on either side of the foundation, especially when the orientation angle is set to 0°. Different methods for predicting scour depth of the MCCBF were applied and discussed.

1. Introduction

Offshore wind energy has significant potential and offers numerous benefits for green energy production. The increased size of individual wind turbines significantly contributes to the economic enhancement of wind power facilities (Li et al., 2022; Tao et al., 2023). Due to the complex environment, i.e., severe sea conditions, the investment costs associated with offshore wind power, however, surpass those of onshore wind power. The cost of offshore wind turbine foundations, also increases with water depth, e.g., a foundation in water depths of 40–50 m would be about twice as expensive as one in depths of 10–20 m (Oh et al., 2018). For this reason, a large wind turbine, with its high efficiency and high output, is more suitable for greater water depth.

The majority of offshore wind turbines are supported by fixed foundations, which include tripod, jacket, monopile, and gravity-based foundations (Wu et al., 2019). Regardless of the type of fixed foundation, local scour has the most significant impact on the stability and safety of offshore wind turbine structures (Ma et al., 2018; Zhang et al., 2021). Recently, local scour around coastal and offshore structures, including offshore wind turbine foundations, has been extensively studied through numerical simulations (Baykal et al., 2015; Saud Afzal et al., 2015; Sogut et al., 2022; Zhang et al., 2020) and physical experiments (Chen and Li, 2018; Chen et al., 2022; Cheng et al., 2022; Dey et al., 2006; Guan et al., 2019; Qi and Gao, 2014; Rudolph and Bos, 2006; Sumer, 2002). Some studies use both numerical and physical model experiments to investigate the maximum scour depth by considering steady current as well as wave-current interaction (Lian et al., 2022; Roulund et al., 2005; Song et al., 2022; Zhao et al., 2010). The studies, however, predominantly focus on monopiles.

The evolution of the wind power industry and its increasing demands have expanded the scope of scour research to encompass different foundation types beyond monopiles. Based on previous research, local scour around more intricate offshore wind foundations has been evaluated. For example, a tripod foundation (Stahlmann and Schlurmann, 2010; Yuan et al., 2017), a pile-group foundation (Ji et al., 2018), a high-rise foundations (Liang et al., 2022), an umbrella suction anchor foundation (Yang et al., 2020), and a jacket foundation (Chen et al., 2022; Lian et al., 2022). A series of flume experiments were conducted to investigate the scour process and equilibrium scour depth around a composite bucket foundation under steady flow, bidirectional flow, and

* Corresponding author.
E-mail address: jfzhang@tju.edu.cn (J. Zhang).

https://doi.org/10.1016/j.coastaleng.2024.104598
Received 9 April 2024; Received in revised form 12 August 2024; Accepted 14 August 2024
Available online 15 August 2024

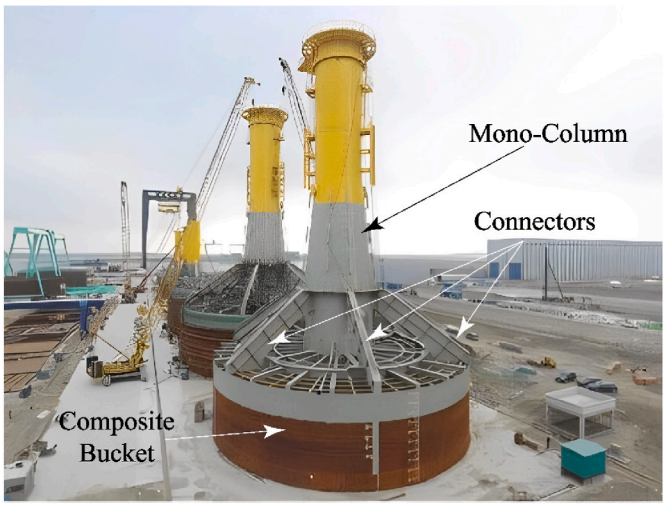

Fig. 1. Photograph of the MCCBF (a large-diameter Mono-Column Composite Bucket Foundation with six connectors).

regular wave-current interaction (Yu et al., 2016, 2019). Regarding the large-diameter mono-column composite bucket foundation with six connectors proposed by Xiao et al. (2020), the potential scour issue has not been investigated yet, apart from the studies on soil-structure interaction (Zhang et al., 2023).

The MCCBF (short for Mono-Column Composite Bucket Foundation) features an all-steel structure (refer to Fig. 1) to address the complexities of geological and hydrodynamic conditions in deep seas. This foundation consists of a mono-column, connectors, and a composite bucket. It addresses the problem of transferring the upper moment and load to the foundation and subsidence susceptible to the traditional gravity foundations (Esteban et al., 2019). Similar to all fixed foundations, the MCCBF's bucket will penetrate into the seabed and stop at a pre-selected depth. The development of scour holes around the bucket may alter the interaction between the structure and the soil, potentially compromising the stability and safety of the MCCBF.

Due to the distinctive structure of MCCBF (i.e., made by the combination of connectors, the mono-column, and the composite bucket), the flow field around it is more complex compared to those of typical foundations such as monopiles. This could lead to significantly different sediment transport around the MCCBF, and the existing empirical formulas for predicting the maximum equilibrium scour depth may not be directly applicable. A comprehensive study on the scour process around the MCCBF is needed. Therefore, physical model experiments were conducted. The effects of different flow patterns, water depths, and orientation angles on the local scour characteristics of the foundation were investigated using model sands based on scale. The study arrangement is as follows: In Section 2, the experimental setup and procedure are presented. The detailed results of the scour tests for the MCCBF are presented in Section 3, along with comparisons and discussions. The conclusions of this study are presented in Section 4.

2. Experiment setup and procedure

2.1. Laboratory facilities and instruments

Local scour experiments were conducted on a model of MCCBF in the large wave and current flume at the State Key Laboratory of Hydraulic Engineering Intelligent Construction and Operation, Tianjin University. The flume, measuring 90 m in length, 2 m in width, and 2 m in height, is equipped with a bidirectional circulating flow system that can generate currents with both velocity and direction that vary over time, such as tidal flow that conforms to sinusoidal changes in flow velocity. A wavemaker equipped with a push plate at the left end of the flume can generate regular Stokes waves. The direction of wave propagation is from the left end to the right end of the whole flume (Fig. 2(a)). The test section, located in the middle of the flume and spanning 21 m in length, features a sand tank with a trapezoidal cross-section that gradually changes from the bottom to the top. The sand tank has a height of 0.3 m, with the bottom section measuring 3 m in length and the top section, after the gradual change, measuring 4 m in length until it reaches the bed surface. On each side of the sand tank, there is a transition section measuring 9 m in length. It consists of a 3 m-long slope with a gradient of 1:10 and a 6 m-long horizontal section. The experimental setup, as depicted in Fig. 2, includes a regular Stokes wave-making system, a wave-absorbing area using the gravel slope. a flow-making system, and a measurement system. Before the model was installed, a wave gauge was placed at the location where the model would be positioned. The incident wave height without the influence of the structure was obtained. The measurement system includes a fixed robotic arm mounted on a three-dimensional (3D) guideway positioning system. It functions as a scour monitoring system for points and profiles, as well as a scour topography measurement system. The Acoustic Doppler Velocimeter (ADV) used in the measurement system also enables underwater topography measurements. The guide planar positioning accuracy of the ADV reaches up to 5 mm, while the scour depth measurement accuracy reaches up to 1 mm.

2.2. Experimental setup

The similarity of sediment transport between the prototype and the model is predicated on the similarity of hydrodynamics. In fact, it is difficult to satisfy both the gravity similarity (i.e., Froude number similarity) and the moving bed resistance similarity (i.e., bed-particle mobility similarity, which can be represented by the same Shields parameter) in scour experiments. Even if these two conditions are met simultaneously, constraints imposed by experimental fields and facilities make it challenging to determine the appropriate geometric scale for scour experiments. In the event that the prototype sediment is fine, the impact of cohesive forces also needs to be taken into consideration.

In summary, when conducting scour experiments under the precondition of Froude number similarity, it is advisable to select coarser and lighter material as the model sand to prevent cohesive forces. This selection should be based on the similarity of critical incipient velocity (u_c) (Wang et al., 2021). Additionally, it is important to consider the similarity between sediment suspension and settlement are taken into consideration based on the similarity of settling velocity (ω). The above idea was adopted in this study to reduce scale effects and minimize the possible error from resistance similarity criterion.

With a median grain size of 0.078 mm, the mixture of the silt and clay at the project site is fine. Therefore, the plastic model sand with a lower density ($\rho_s = 1050$ kg/m^3) and a larger median grain size ($d_{50} = 0.16$ mm) was used in the experiments. Scour development will be effectively accelerated by utilizing model sand, leading to time savings around the foundation. The prototype scour depth can be directly obtained from experimental results and the corresponding geometric scale. The geometric scale was chosen as 1:50, while the scales for time and velocity were set at 1:7.07 to fulfill Froude number similarity. Both the incipient velocity and settling velocity follow the scale of velocity simultaneously. A comprehensive comparison of velocities between the model sand and the prototype sediment is provided in Table 1. The critical incipient velocity and settling velocity of both prototype sand and model sand were determined through two preliminary experiments. Incipient sediment motion on a flat sand bed in a small flume was observed at various flow velocities to obtain the depth-averaged critical velocity. The settling process of sediment particles in a settling tube was captured frame-by-frame using a high-speed camera. The displacement-time curves were used to determine the settling velocities of different sediment particles in water, and the volume-averaged settling velocity of all particles was then calculated.

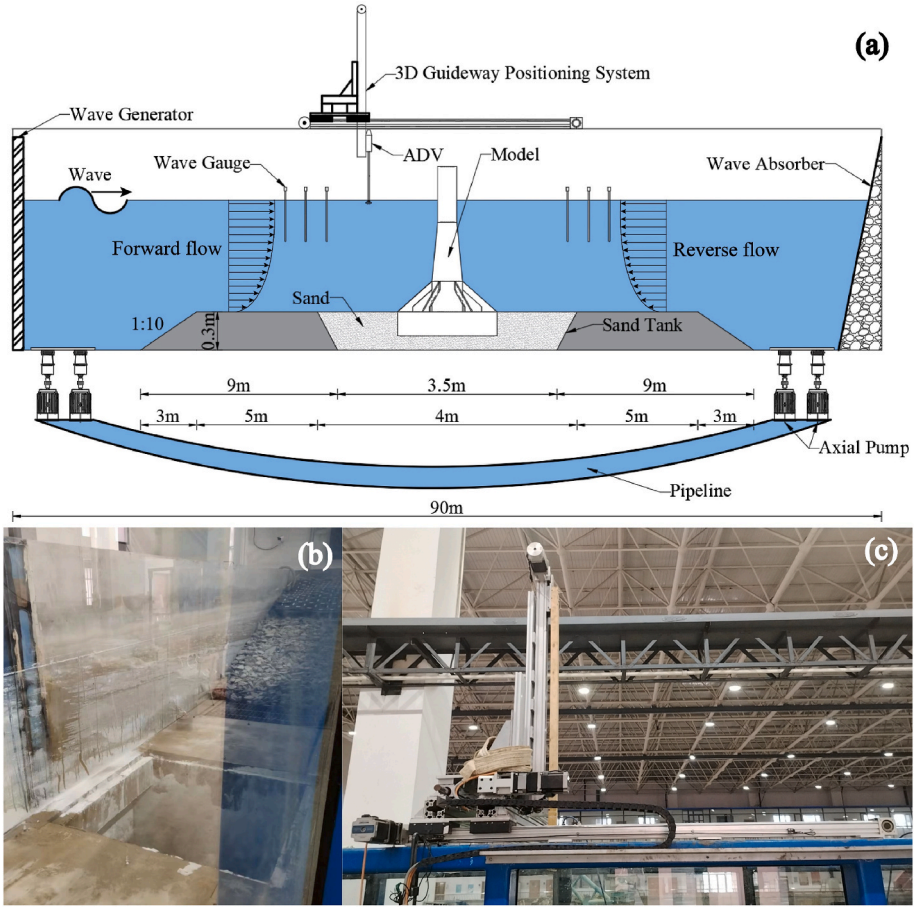

Fig. 2. Experimental set-up (a) sketch of experimental set-up; (b) sump pit for pumps; (c) 3D guideway positioning system.

Table 1
Comparison of critical velocities during incipient motion and settling velocities between prototype sand and model sand.

	Prototype sand	Model sand	Actual scale	Theoretical scale	Relative error
Critical velocity u_c (m/s)	0.583	0.085	6.86	7.07	2.97%
Settling velocity ω(mm/s)	3.130	0.440	7.11	7.07	0.57%

The laboratory model of MCCBF followed a length scale of 1:50. All MCCBFs currently deployed in the Yangjiang wind farm have adopted connectors with the structural configuration illustrated in Fig. 3. The model was positioned in the middle section of the flume, approximately 45 m away from both ends of the flume. When the flume was empty without water, the composite bucket was gradually sunk into the model sand bed using manual loading through the ventilation of small air holes on its surface, until the top surface of the composite bucket was at the same elevation as the sand bed. The submergence depth of the model foundation is 19 cm. During the experiments, the model was kept stable by the composite bucket foundation rather than being fixed to the ground or other supports. Nevertheless, this still cannot exactly replicate the installation and operation processes of MCCBFs in the field. The experimental conditions can be found in Table 2, which included testing two distinct orientation angles: 0° and 30° (Fig. 4). The study evaluated two water depths (0.8 m and 0.82 m) and three different design depth-averaged flow velocities (0.12 m/s, 0.15 m/s, and 0.18 m/s). The tested flow patterns included unidirectional flow, semidiurnal tidal flow, and wave-current interaction. The tidal period is 106 min calculated by the time scale. The tidal velocity follows a sinusoidal pattern, with the peak velocity aligning with the design velocity. During the experiment under wave-current interaction, the direction of waves and currents were same.

In order to determine the time when the local scour is at its maximum and reaches a stable condition, a comprehensive monitoring system was established around the model (Fig. 5). The system consisted of 12 monitoring points and 4 monitoring profiles, positioned according to the structural characteristics of the foundation. The monitoring points were positioned 5 cm away from the model's edge, evenly distributed at 30° intervals around the circumference. Each point was assigned a serial number and position corresponding to the 12 h on a clock face when facing the flow direction. Additionally, two monitoring profiles were arranged perpendicular to the flow direction and two parallel to it. These profiles allowed for the observation of scour development around the model, with 45 points spaced 2 cm apart on each profile.

The measurement of all monitoring points and profiles is conducted at 10-min intervals. During each measurement period, it was not feasible to collect data simultaneously from the monitoring points and profiles due to the limitation in the number of instruments. Consequently, flow generation was stopped, and the scour experiment was continued after the measurement was completed (approximately 10 min later). At all 12 monitoring points, if the differences in scour depth at each point do not exceed 5%–10% across three consecutive measurements, and the rate of scour depth increase gradually decreases over time or even shows minor fluctuations, it can be concluded that equilibrium has been reached. Simultaneously, it should be observed that the shapes of the four profiles do not show significant changes or only fluctuate within a small range. Following the scour equilibrium, the equilibrium scour topography was

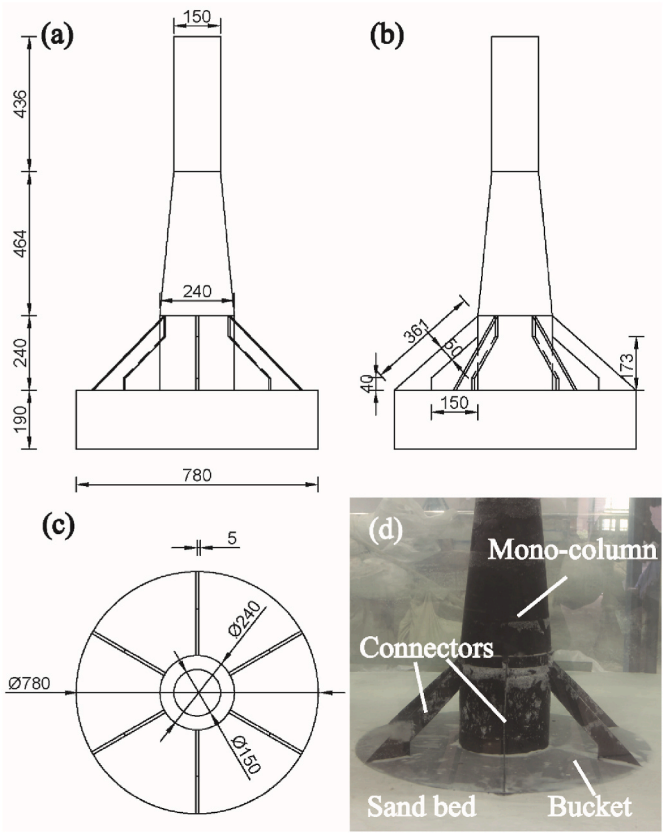

Fig. 3. Model of the MCCBF: (a) front view (mm); (b) side view (mm); (c) top view (mm); (d) photograph.

Table 2
Experimental conditions.

Test NO.	α(°)	h(m)	u (m/s)	T_{tide} (min)	H_m, T_m
1	30	0.82	0.15	–	–
2	30	0.82	0.15	106	–
3	30	0.8	0.18	–	–
4	30	0.8	0.18	106	–
5	0	0.82	0.12	–	–
6	0	0.82	0.15	–	–
7	0	0.82	0.15	106	–
8	0	0.8	0.18	–	–
9	0	0.8	0.18	106	–
10	0	0.82	0.15	–	0.04m 1.36s

measured. The acoustic Doppler velocimeter (ADV) and a 3D positioning system were used to record the coordinates and scour depths around the bucket, which had dimensions of approximately 1.5m in width and 2.5m in length. The collection of local scour data requires a minimum of 12 h. After this period, the data can be processed to obtain the scour contour.

After one measurement, the water drained out slowly. Subsequently, the location where the maximum scour depth occurred was measured with a ruler. This served as a confirmation of the acoustic measurements. All experimental conditions mentioned in Table 2 were conducted in a similar manner.

3. Results and discussion

The local scour of the MCCBF involves intricate interactions among water flow, the sand bed, and the various structural components. To describe and analyze the experimental findings, A simple schematic is shown (Fig. 6) to illustrate the main flow around the MCCBF at different orientation angles, drawing from both experimental observations of sediment transport around the model and prior scholarly studies about monopiles (Sumer, 2002). The flow effects mainly influenced by the mono-column or the connectors are shown using hollow arrows or solid black arrows, respectively.

It is found that streamline contractions on both sides of the mono-column cannot directly influence the sand bed as they are concealed by the surface of the bucket (Fig. 6). The relative position of the connector to the mono-column varies with different orientation angles. While differences in sediment transport behind the mono-column can be observed in the experiments at two orientation angles, the specific effects of the connector on vortex generation behind the mono-column cannot be obtained from the present study. It necessitates further investigation using methods like numerical simulations or particle image velocimetry (PIV). Around the connectors (Fig. 4), such as (2) and (5) at $\alpha = 30°$, and (1), (2), (4), and (5) at $\alpha = 0°$, there are small lee-wake vortices and streamline contraction.

Some tests have identical orientation angles and show similar scour evolution. Although the flow velocities are different (e.g., Test2 and Test4; Test5, Test6, and Test8), the analysis of scour development and equilibrium topography focuses on cases with higher flow intensities. Some results of scour development at small flow velocities are placed in the appendix. Equilibrium scour topography contours are provided for all tests.

3.1. Development of scour depth with time

For the steady flow in Test 3 (with the orientation angle $\alpha = 30°$, water depth $h = 0.8$ m, and steady flow velocity $u = 0.18$ m/s), there is an initial rapid scour evolution in scour depth at points (e.g., ③, ⑤, and ⑦ in Fig. 7) adjacent to the downstream connectors (2), (3), and (4). This rapid increase is attributed to the influence of streamline contraction and lee-wake vortices, resulting in a surge of over 4 cm within 30

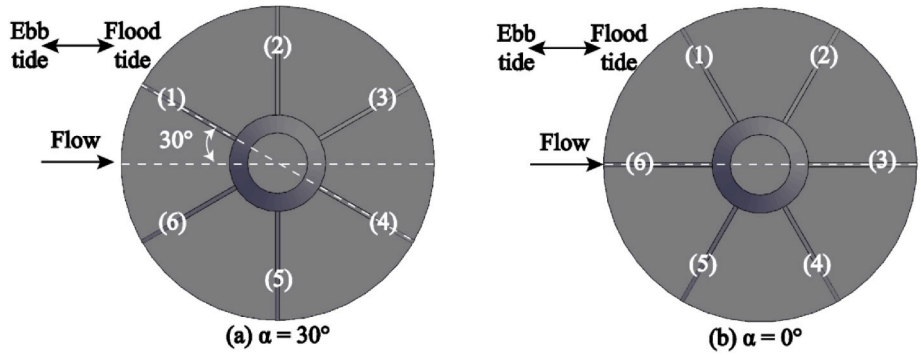

Fig. 4. Layout of connectors number and current direction around the single-column composite cylinder foundation under different angles; (a) $\alpha = 30°$; (b) $\alpha = 0°$.

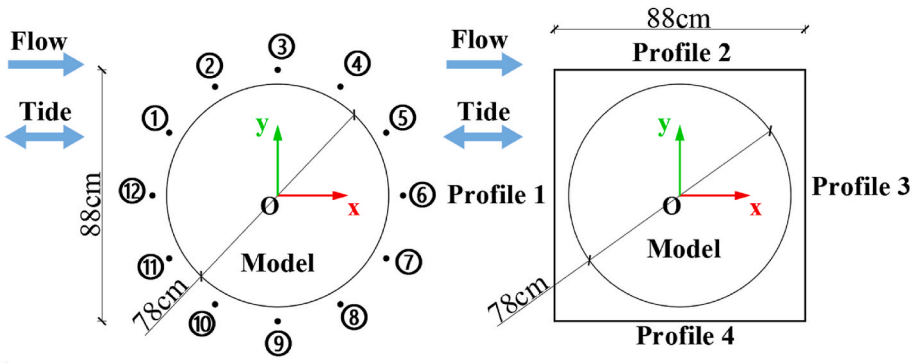

Fig. 5. Location of monitoring points and profiles; (a) 12 monitoring points; (b) 4 monitoring profiles.

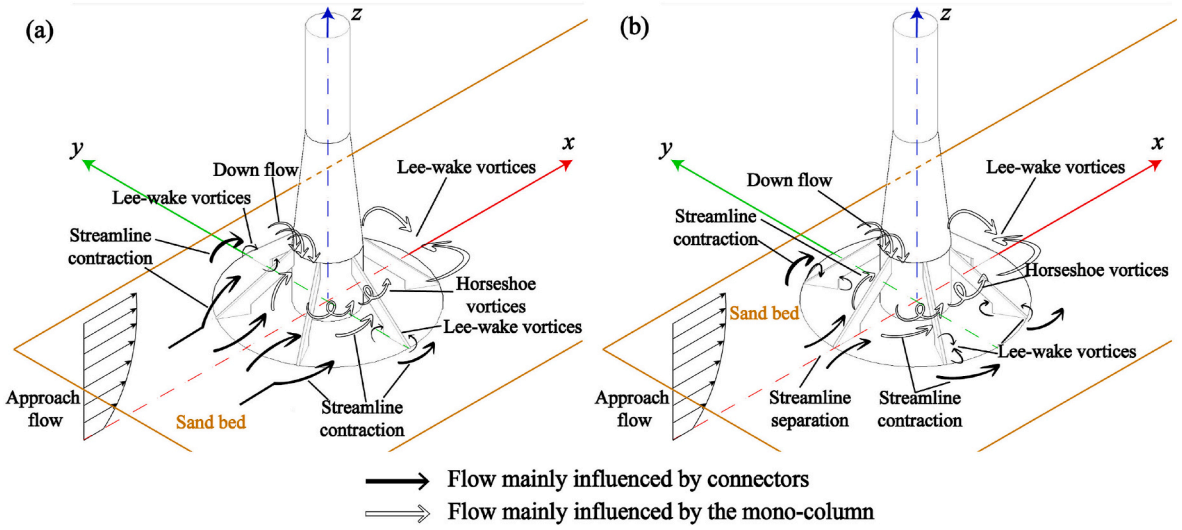

Fig. 6. Schematic diagram of flow characteristics around a MCCBF penetrated in the sand bed; (a) $\alpha = 30°$; (b) $\alpha = 0°$.

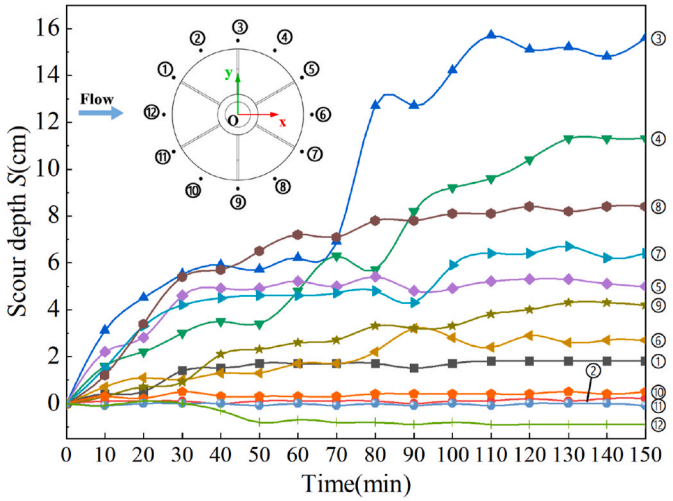

Fig. 7. Development of scour depth over time at 12 monitoring points of Test 3 ($\alpha = 30°$, $h = 0.8$ m, $u = 0.18$ m/s).

min. The scour depth at point ⑨ did not show a similar trend to the symmetrical point ③. While points around the upstream connectors (1) and (6), such as ① and ⑪, exhibit minimal changes in scour depth. Notably, siltation of sand is observed at point ⑫. The scour depth at the majority of measuring points shows steady development after 100 min. All points reach equilibrium after 150 min.

Fig. 8 illustrates the development of scour over time for four monitoring profiles in Test 3, with profiles displayed at 20-min intervals for clarity. Profile 1 (Fig. 8 (a)) confirms the small scour depth observed at points ① and ⑪, and the siltation at point ⑫. Profiles 2 (Fig. 8 (b)) and 4 (Fig. 8 (d)) depict the development of scour near connectors (2) and (5), positioned perpendicular to the flow direction. Scour occurs first at the locations of connectors (2) and (5), initiating and gradually developing downstream, steadily deepening, and reaching scour equilibrium with a maximum depth of 17 cm. Profile 3 (Fig. 8 (c)) shows the downstream development of scour. Under the influence of a mono-column and connectors, two relatively symmetrical independent scour holes gradually form.

For the scour asymmetry that occurs in Test3, such as in points ③ and ⑨, Profiles 2 and Profiles 4, etc., it is evident that the development of scour depth over time on both sides of the model is not entirely symmetrical. Unlike the scour holes of a monopile, the significantly accelerated flow around the mono-column does not directly impact the sand bed because of the sheltering effect of the bucket. The gradual exposure of the bucket can also impact the flow and the development of scour. The asymmetry of the scour is influenced by where and when the bucket is exposed. If only the downstream portion of the composite bucket is exposed from the sand bed while the upstream portion remains buried, there are no conditions for streamline contractions that could significantly influence the scour on both sides of the bucket. There is no guarantee that the properties of the sand bed surrounding the model will be perfectly homogeneous and symmetrical in the laboratory tests. In fact, all of the above factors combine to amplify asymmetric scour not only in Test 3 but also in other cases. In the case of composite bucket

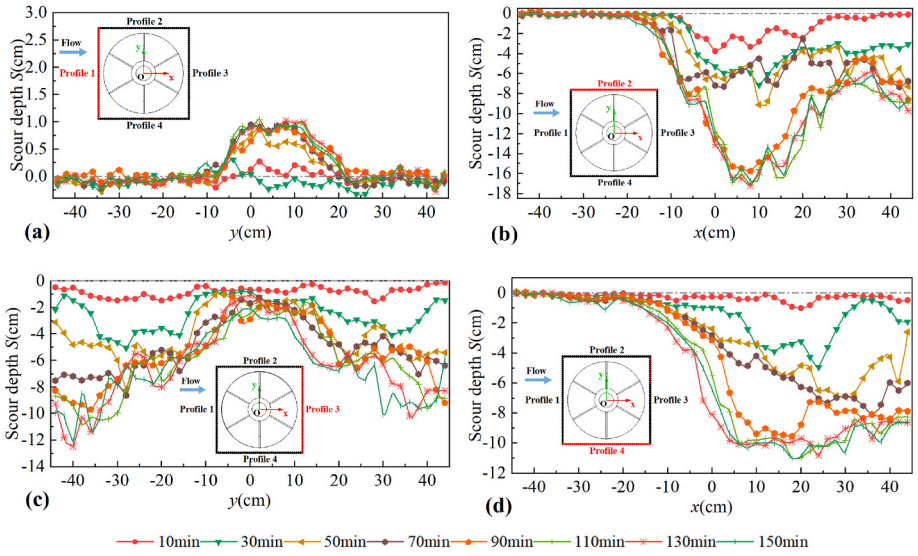

Fig. 8. Development of scour depth over time in the 4 monitoring profiles of Test3.

foundations buried in the sand bed with a large foundation area, Yu et al. (2016) also observed scour asymmetries at higher flow velocities in their experiments.

For the tidal flow in Test 4 (with the orientation angle $\alpha = 30°$, water depth $h = 0.8$ m, and maximum tidal current velocity $u = 0.18$ m/s), the graph in Fig. 9 shows the variation in scour depth over half a tidal period. Due to the alternating sediment transport caused by periodic changes in flow direction and velocities, all points show fluctuations with an overall increasing trend in scour depths. During the first flood tide (0–53 min), noticeable scour is evident at most points, excluding points ①, ⑪, and ⑫. Subsequently, the scour rate gradually plateaued. Due to the inherent symmetry of the structure, the upstream of the model transitioned to its downstream at the first ebb tide (53–106 min). Scour gradually occurred at points ① and ⑫. The scour reaches equilibrium at all monitoring points after five tidal periods (530 min). Similar to the unidirectional flow, the scour depth at points near connectors (2) and (5) was greater, although it was less than that observed in the unidirectional flow.

During the initial flood tide, there is no scour at profile 1 (Fig. 10(a)), but scour gradually emerges during the subsequent ebb tide. In contrast,

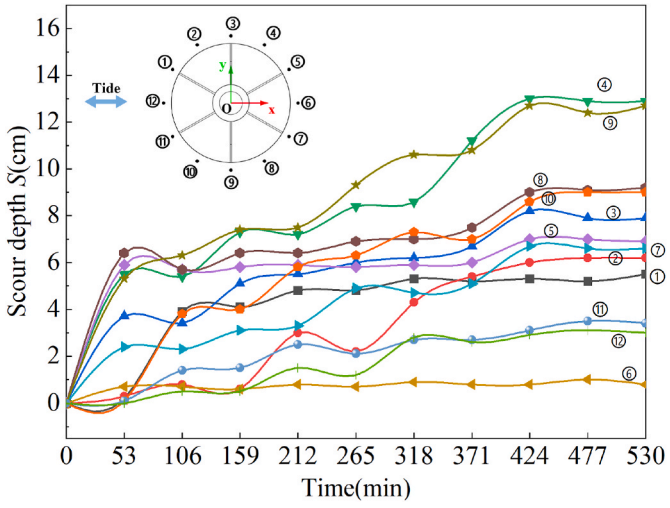

Fig. 9. Development of scour depth over time at 12 monitoring points of Test 4 ($\alpha = 30°$, $h = 0.8$ m, $T_{tide} = 106$min, $u_{max} = 0.18$ m/s).

profile 3 (Fig. 10(c)) experienced scour during the first flood tide, which intensifies rapidly during the subsequent second flood tide. The presence of the mono-column and connectors leads to the gradual formation of two distinct scour holes in profiles 1 and 3, respectively. Notably, scour holes in profile 3 are larger and deeper, reaching a maximum depth of 10 cm. Profiles 2 (Fig. 10 (b)) and 4 (Fig. 10 (d)) depict the development of scour due to the reciprocating tidal flow at connectors (2) and (5), which are positioned perpendicular to the flow direction. During the first flood tide, scour holes develop downstream of the flood tide (near points ④ and ⑧), while no substantial scour occurs upstream (near points ② and ⑩). As the first ebb tide commences, scour holes develop downstream of the ebb tide at these points (near points ② and ⑩), altering the flat sand bed profile. Scour depths increase in profiles 2 and 4 both upstream and downstream, regardless of whether it is flood tide or ebb tide. The maximum scour depth can reach 17 cm before reaching scour equilibrium.

In Test 8, when the orientation angle is set at 0°, the scour depth increases rapidly under steady flow at monitoring points (as shown in Fig. 11) close to connectors (1), (2), (4), and (5) that have a particular intersection angle in relation to the flow direction (e.g., Point ④, ⑤, ⑧, and ⑨). This phenomenon is attributed to the influence of streamline contraction and lee-wake vortices, similar to Test 3. Meanwhile, the scour depth experiences less variation at monitoring points near connectors (3) and (6), which are parallel to the flow direction. All monitoring points show fluctuations, with an overall increasing trend in scour depths. The scour depth stabilizes at most points after 110 min and reaches scour equilibrium after 140 min. To verify whether the sudden scour observed in front of the bucket after 80 min (i.e., points ①, ⑪, and ⑫) had reached equilibrium, an additional 20-min scour test was conducted and shown in Fig. 11. It can be seen that at a flow velocity of 0.18 m/s, the scour in front of the bucket has already reached equilibrium. The scour did not further develop to expose the upstream portion of the bucket beneath the sand bed.

For all profiles except profile 1 (Fig. 12(a)), rapid scour depth development occurs within the initial half-hour period. Profiles 2 (Fig. 12 (b)) and 4 (Fig. 12 (d)) demonstrate the development of scour near connections (1), (2), (4), and (5) positioned at a specific angle relative to the flow direction. The scour depth of the profiles changes significantly at two specific locations due to the influence of adjacent connectors ((1) and (2); (4) and (5)). Within the first 40 min, scour development near downstream connectors (2) and (4) exhibited accelerated rates. Subsequently, scour development near connectors (1) and (5) accelerated. Profile 2 and profile 4 gradually stabilize as two deeper

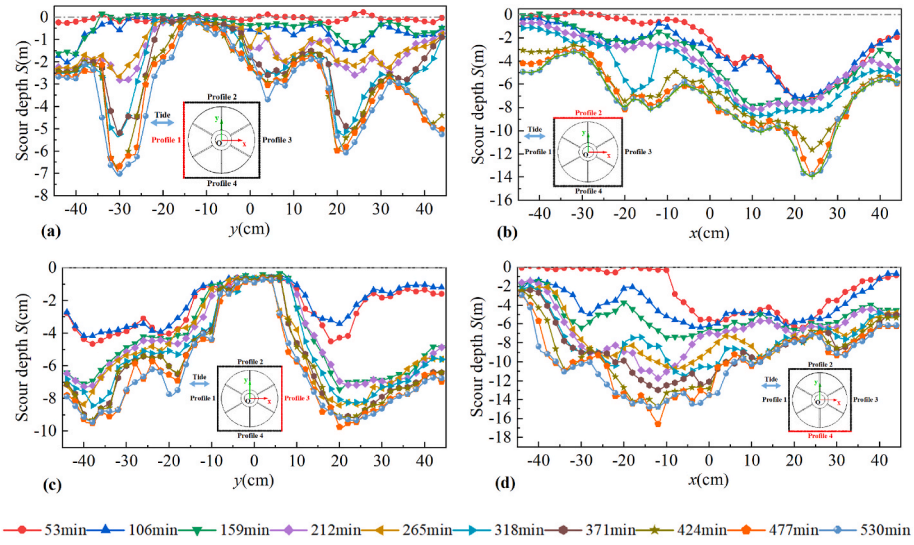

Fig. 10. Development of scour depth over time in the 4 monitoring profiles of Test4.

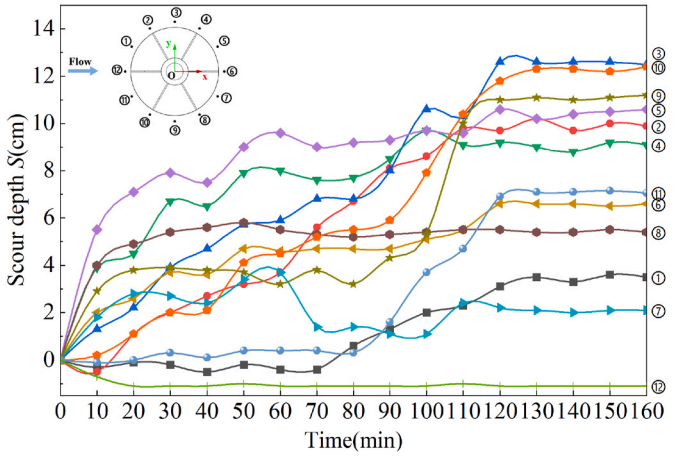

Fig. 11. Development of scour depth over time at 12 monitoring points of Test 8 ($\alpha = 0°$, $h = 0.8$ m, $u = 0.18$ m/s).

scour holes merge to form a larger one. These profiles display an overall upstream movement tendency in scour development. This behavior is highlighted by the sudden emergence of two larger scour pits in profile 1 after 100 min, marking a significant deviation from observations in Test 3. Furthermore, the scour reached equilibrium after 140 min, without further development that would fully expose the upstream portion of the bucket. It corroborates the conclusions previously obtained from Fig. 11. Nonetheless, at higher flow velocities (greater than 0.18 m/s), there is a possibility that continued exposure of the bucket in the upstream region may further intensify the scour on both sides of the structure. Finally, profile 3 (Fig. 12(c)) shows the downstream development of two distinct scour holes until reaching scour equilibrium.

In Test 9 with tidal flow and a orientation angle of 0°, the reciprocal sediment transport resulting from periodic changes in flow direction and velocity leads to varying scour depths at all locations, as depicted in Fig. 13. A general trend of increasing scour depth is evident, with slight siltation observed during the initial flood tide phase (0–53 min) at points upstream of the model, such as ⑩, ⑪ and ⑫, while the remaining points exhibit scouring. As the first ebb tide approaches (53–106 min), all points exhibit scouring due to the symmetry of the foundation. Scour equilibrium is reached after five tidal periods. Similar to Test 8, points

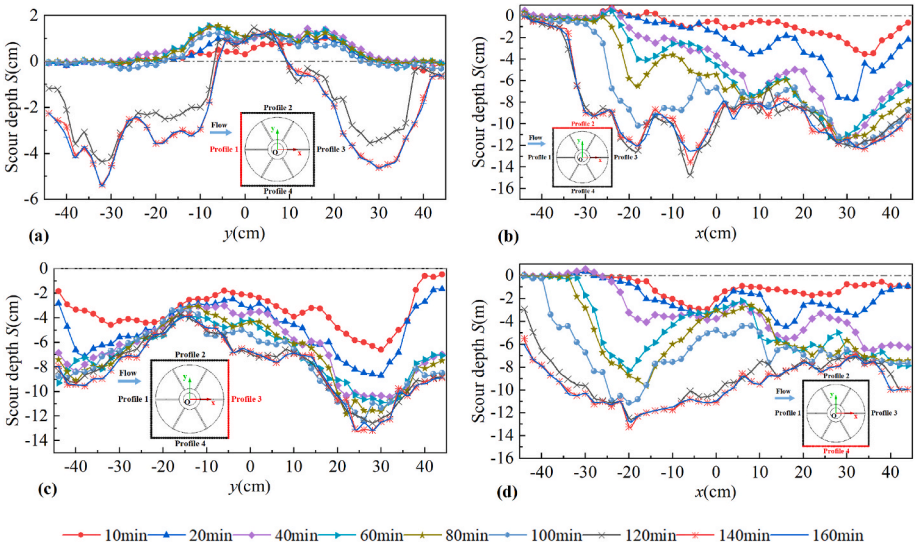

Fig. 12. Development of scour depth over time in the 4 monitoring profiles of Test8.

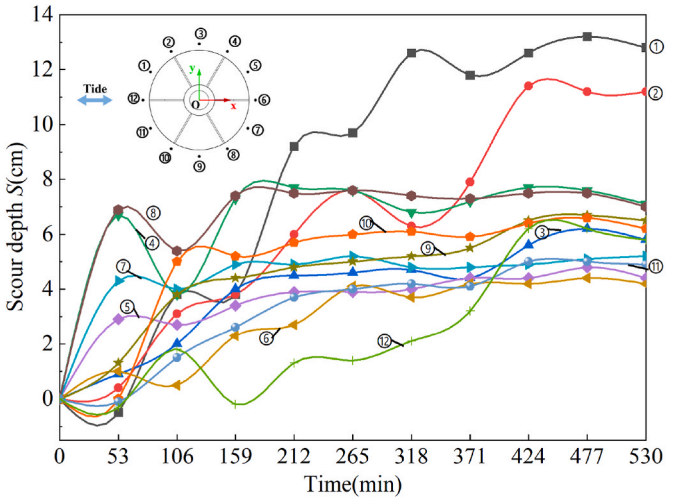

Fig. 13. Development of scour depth over time at 12 monitoring points of Test 9 ($\alpha = 0°$, $h = 0.8$ m, $T_{tide} = 106$min, $u_{max} = 0.18$ m/s).

near connectors (1), (2), (4), and (5) demonstrate a higher scour depth of approximately 13 cm, but lower than that observed in Test 8.

Profile 1 in Fig. 14(a) exhibits no scour during the initial flood tide, but experiences scour during the subsequent ebb tide, with significant scour occurring after the second ebb tide. This results in the gradual formation of two distinct scour holes with a maximum depth of 15 cm. Profile 3 in Fig. 14(c) displays considerable scour during the first flood tide, approaching scour equilibrium profiles after the second flood tide. Profiles 2 (Fig. 14(b)) and 4 (Fig. 14(d)) illustrate the development of scour in the sand bed near connectors (1), (2), (4), and (5) due to tidal flow. Similar to Test 8, the scour depth near the connectors is impacted, leading to the formation of scour holes both upstream and downstream. Ultimately, the scour holes around the connectors in each profile merge to create a larger scour hole. As the scour approached equilibrium, the shape of the scour holes at the four profiles remained generally stable. There is even slight sand backfilling during the final ebb flow (at 530 min), causing a fluctuation in scour depth.

3.2. Equilibrium scour topography

After reaching scour equilibrium in each test, the scour topography was measured and subsequently charted using the scour topography measurement system. For Test 3 (with the orientation angle of $\alpha = 30°$, water depth $h = 0.8$ m, and steady flow velocity $u = 0.18$ m/s), the upstream sand bed of the composite bucket remains mostly unaffected under steady flow conditions. There was slight siltation observed with a thickness of approximately 2 cm. Only slight scour is observed at the upstream connectors (1) and (6). The main current responsible for scour has limited influence on the upstream region of the composite bucket due to its cover. Even in the upstream region, approximately 1–2 times the diameter from the center of the mono-column, the bed shear stress is lower than that on a flat bed without structures (Roulund et al., 2005). The reduced shear stress in this area allows sediment transported by the upstream flow to accumulate. However, significant scour occurs near connectors (2) and (5), which are perpendicular to the flow (Fig. 15(a)). Noteworthy streamline contraction and lee-wake vortices are present. The scour holes gradually merge with other scour areas downstream, forming two distinct and symmetrical scour holes along the flow. These scour holes have a length of up to approximately 175 cm. They feature a greater scour depth upstream and a smaller depth downstream, with a maximum scour depth of 17.6 cm (Fig. 15(b)). The findings of equilibrium scour topography align with the analysis of characteristic measuring points and profiles discussed in the previous section.

For the tidal flow in Test 4 (with the orientation angle $\alpha = 30°$, water depth $h = 0.8$ m, and maximum tidal current velocity $u = 0.18$ m/s), substantial scour is observable both upstream and downstream. A noticeable sand ridge forms along the central axis of the structure, aligned with the flow direction, which separates the scour holes on either side of the foundation. While the scour holes are symmetrical distribution along the flow direction, the scour depth is asymmetrical. Similar to scour patterns observed in unidirectional steady flow, severe scour occurs near the connectors (2) and (5), which are perpendicular to the flow. However, during flood tide, one deeper scour hole is positioned downstream of the foundation. And during ebb tide, another deeper scour hole emerges downstream. Scour occurs on both sides of the foundation, gradually exposing the bucket beneath the sand bed. Additionally, the presence of the bucket further amplifies the extent of scour (Fig. 16(a)).

The scour phenomenon exhibits an asymmetrical pattern both upstream and downstream of the foundation. Initially, during the first

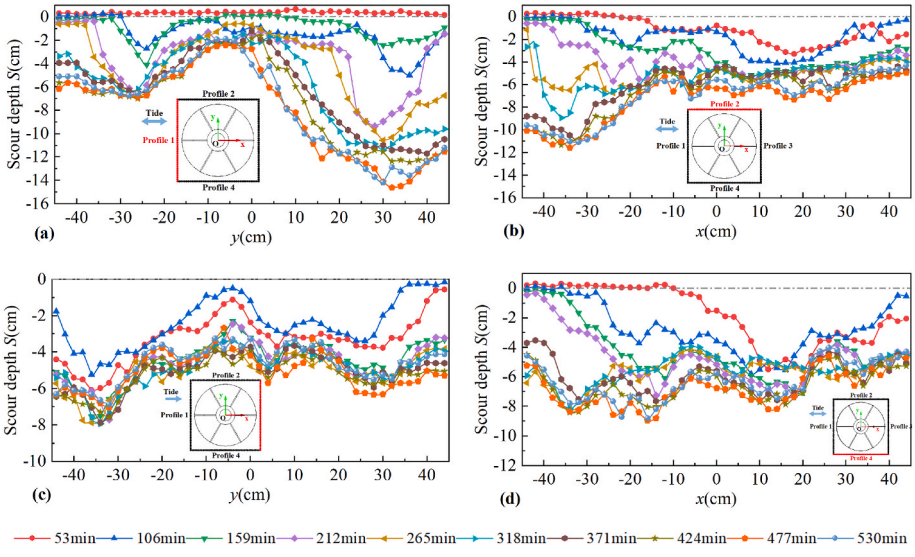

Fig. 14. Development of scour depth over time in the 4 monitoring profiles of Test 9.

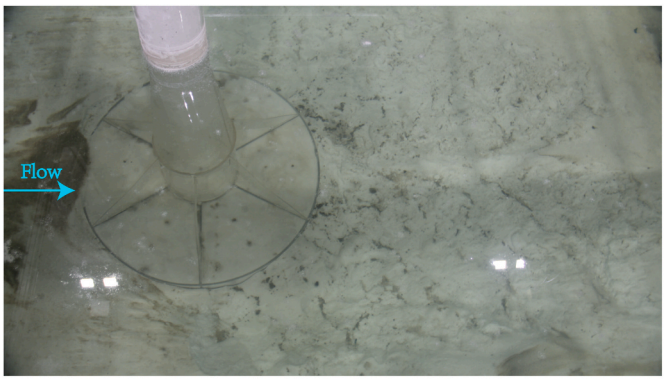

(a)

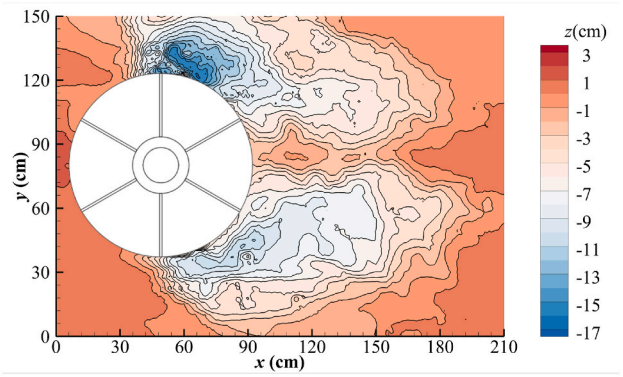

(b)

Fig. 15. Equilibrium scour topography of Test 3: (a) Photography; (b) Contour.

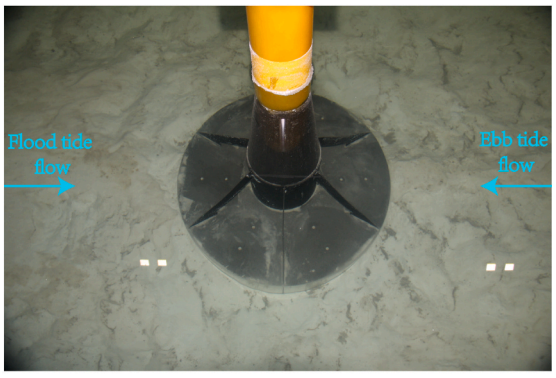

(a)

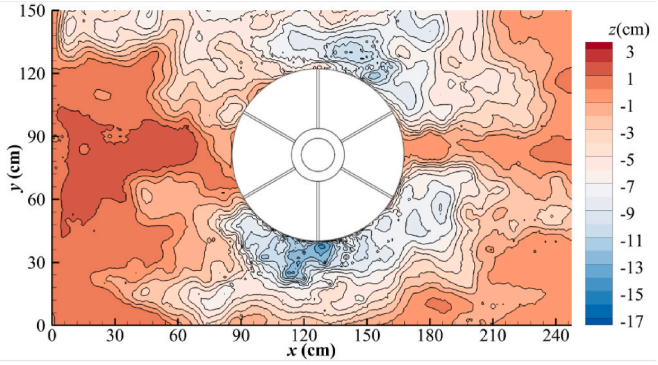

(b)

Fig. 16. Equilibrium scour topography of Test 4: (a) Photography; (b) Contour.

flood tide, the development of scour holes near the bucket's downstream area impacts the flow dynamics for the subsequent ebb tide. This results in the flow passing through the expanded cross-sectional area of the scour holes rather than the flat bed before reaching the foundation. Consequently, this modification in flow velocity affecting the foundation weakens the downstream scour development by the ebb tide. In the subsequent second flood tide, the upstream sand bed also deviates from being flat due to the existing scour holes, leading to a corresponding decrease in flow velocity. These combined factors limit the growth of the maximum scour depth when compared to Test 3. Consequently, the maximum scour depth recorded in Test 4 is 16.8 cm (as illustrated in Fig. 16(b)), very close to that observed in Test 3. Despite this, the scour holes in Test 4 exhibit greater length along the flow direction, extending to approximately 245 cm after reaching scour equilibrium.

In the Test 8 (with the orientation angle $\alpha = 0°$, water depth $h = 0.8$ m, and steady flow velocity $u = 0.18$ m/s), the scour topography matched previous results of monitoring points and profiles. Combining the experimental observations and the analysis from Figs. 11 and 12, it was observed that the flow dynamics were more intricate near specific connectors ((1) and (5); (2) and (4)). Lee-wake vortices and streamline contraction are present near connectors that have certain angles to the flow direction. Two separate scour holes initially formed in this region and gradually connected along the flow, resulting in deeper scour depth between these connectors. As the bucket beneath the sand bed was exposed, creating a narrow channel by combining with the scour holes, this process led to accelerated flow, intensified scour depth near the connectors, and expanded downstream scour holes. Scour depth decreased further from the foundation. Similar to an orientation angle of 30°, symmetrically distributed scour holes on both sides connected to form a horseshoe-shaped scour hole (Fig. 17(a)). In the areas upstream and downstream near connectors (3) and (6), the bucket beneath the sand bed is exposed. The scour hole reached a maximum length of 222 cm and a maximum depth of 17.9 cm. Compared to Test 3, the extent of scour is significantly larger, while the scour depth is quite similar in Test 8.

For the tidal flow in Test 9 (with the orientation angle $\alpha = 0°$, water depth $h = 0.8$ m, and maximum tidal current velocity $u = 0.18$ m/s), significant scour is observed both upstream and downstream of the foundation (Fig. 18(a)), especially near the two pairs of connectors ((1) and (5); (2) and (4)) with specific angles to the flow direction. The flow conditions in these areas are complex, leading to severe scour. The scour holes on either side of the foundation continuously grow and merge with each other due to the periodic flow. The bucket under sand bed is completely exposed. The distribution of scour holes is roughly symmetrical along the flow, but the scour depths are not symmetrical. The area of larger scour depth is located upstream of the foundation between connectors (1) and (6) at flood tide. The scour holes exhibit asymmetry upstream and downstream of the model due to the combined effects of the connectors and the bucket.

Based on the experimental observations and the analysis of Figs. 13 and 14, there is an acceleration of the flow near connectors (1) and (2) (or (4) and (5)) during the initial flood tide. Two relatively independent scour holes appear around connectors and then gradually merge into one. This results in the exposure of a buried bucket under the sand, creating a narrow flow channel when combined with the scour holes, similar to what was observed in Test 8. However, the downstream scour hole had not fully developed by the end of the first flood tide. The acceleration of the water flow through the channel promoted the scouring of the foundation downstream (upstream of the flood tide) during the subsequent first ebb tide. When the second flood tide arrives, the scour hole has already presented upstream. As the flow passes through the

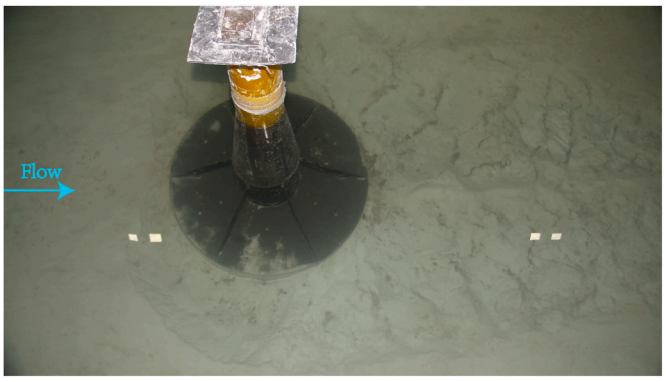

(a)

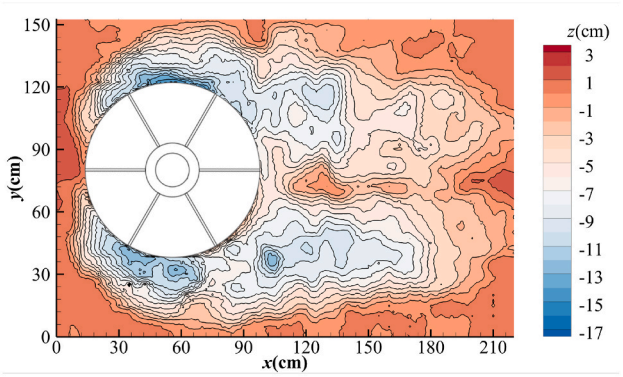

(b)

Fig. 17. Equilibrium scour topography of Test 8: (a) Photography; (b) Contour.

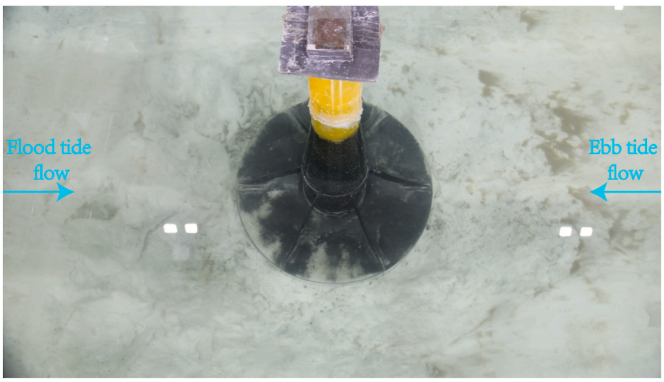

(a)

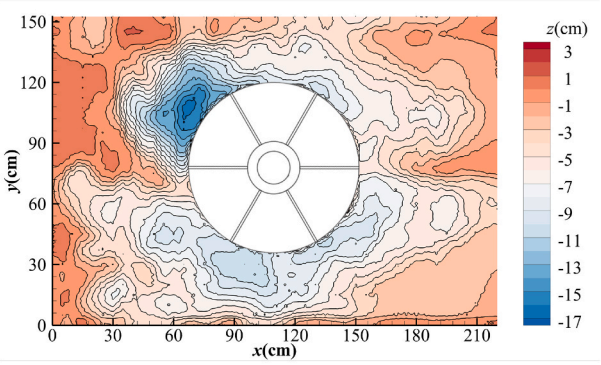

(b)

Fig. 18. Equilibrium scour topography of Test 9: (a) Photography; (b) Contour.

enlarged section, the flow velocity decreases slightly, which reduce the scour impact downstream. A greater scour depth is achieved between connectors (1) and (6) until scour equilibrium is reached. The maximum length of the scour holes is 232 cm, with a maximum depth of 17.2 cm (Fig. 18(b)). The scour depth is slightly greater than the result of Test 4 but slightly less than that of Test 8. In fact, at a depth-averaged flow velocity of 0.18 m/s, the scour depths across the three tests are very close.

In the upcoming discussion, the shape of the equilibrium scour topography for the remaining tests is illustrated for comparison and analysis (see Fig. 19). Additionally, further information on scour is provided, such as the maximum length of the scour holes in the flow direction (L), the maximum length perpendicular to the flow direction (W), and the maximum depth of scour (S_{max}) once equilibrium is reached (refer to Table 3).

4. Discussion

4.1. Effect of flow velocity on scour characteristics

The experiments were conducted using three different flow velocities: 0.12 m/s, 0.15 m/s, and 0.18 m/s. Variations in water depth were not considered in the analysis due to close water depths. The flow velocities primarily impacted the flow intensity around the connectors, mono-column, and exposed bucket on the seabed. The equilibrium scour topography contours of the tests under the same conditions except for the flow velocities were compared, i.e., Test 1 (Fig. 19(a)) and Test 3 (Fig. 15(b)); Test 2 (Fig. 19(b)) and Test 4 (Fig. 16(b)); Test 5 (Fig. 19(c)), Test 6 (Fig. 19(d)), and Test 8 (Fig. 17(b)); Test 7 (Fig. 19(e)) and Test 9 (Fig. 18(b)). It is found that higher flow velocities lead to increased local scour depth. The scour area expanded from the connectors downstream, sometimes reaching upstream, causing the location of maximum equilibrium scour depth to shift upstream. At higher flow velocities, the scour depth remained asymmetrical, but the distribution of scour holes became more symmetrical. This asymmetry could be due to non-uniform initial sand bed conditions around the foundation in the physical model experiments, which were intensified by higher flow velocities. Yu et al. (2016) also noted similar asymmetrical scour patterns in their study on a composite bucket foundation.

4.2. Effect of orientation angles on scour characteristics

All tests were conducted with two orientation angles, specifically 30° and 0°. The variation in orientation angles primarily impacts the flow field around the connectors, as depicted in Fig. 6. Comparative analyses of equilibrium scour topography contours were carried out for various test scenarios, including Test 1 and Test 6, Test 2 and Test 7, Test 3 and Test 8, as well as Test 4 and Test 9, as detailed in Section 3.3.1. When the orientation angle is set at 30°, the primary scouring in the model occurs around connectors (2) and (5) that are perpendicular to the flow direction, and around connectors (3) and (4) (or (1) and (6) during ebb tide), gradually extending downstream or upstream from connectors (2) and (5). Conversely, when the orientation angle is at 0°, scour predominantly takes place around connectors (1) and (5), as well as (2) and (4). A notable increase in both the intensity and extent of scour is observed around the downstream pair of connectors, specifically (1) and (5) under steady flow and flood tide conditions, and (2) and (4) during ebb tide. It is found that the maximum scour depth at orientation angle of 0° consistently surpasses that observed at orientation angle of 30° under similar conditions in Table 3. This phenomenon is attributed to the formation of two initial scour holes near connectors (1) and (2) (or

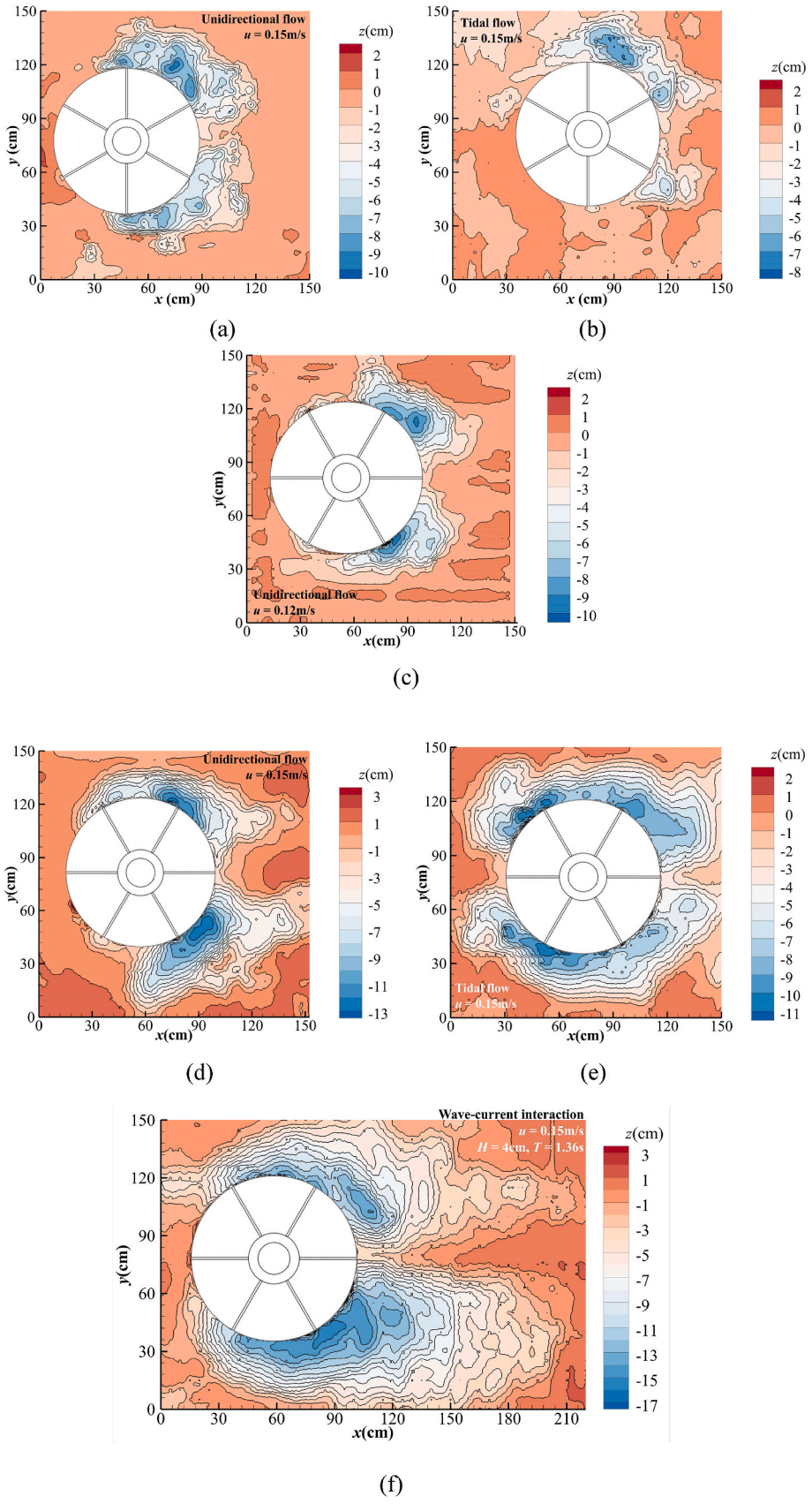

Fig. 19. Contour plots of equilibrium scour topography: (a) Test 1 ($\alpha = 30°$, $h = 0.82$ m, $u = 0.15$ m/s); (b) Test 2 ($\alpha = 30°$, $h = 0.82$ m, $T_{tide} = 106$min, $u_{max} = 0.15$ m/s); (c) Test 5 ($\alpha = 0°$, $h = 0.82$ m, $u = 0.12$ m/s); (d) Test 6 ($\alpha = 0°$, $h = 0.82$ m, $u = 0.15$ m/s); (e) Test 7 ($\alpha = 0°$, $h = 0.82$ m, $T_{tide} = 106$min, $u_{max} = 0.15$ m/s); (f) Test 10 ($\alpha = 0°$, $h = 0.82$ m, $T_m = 1.36$s, $H_m = 0.04$m, $u = 0.15$ m/s).

Table 3
Experimental results for local scour around a single-column composite cylinder foundation.

Test NO.	$\alpha(^\circ)$	h(m)	u (m/s)	T_{tide} (min)	H_m, T_m	L(m)	W(m)	S_{max}(m)
1	30	0.82	0.15	–	–	0.85	0.53	0.105
2	30	0.82	0.15	106	–	0.93	0.64	0.081
3	30	0.8	0.18	–	–	1.75	0.84	0.176
4	30	0.8	0.18	106	–	2.45	0.83	0.168
5	0	0.82	0.12	–	–	1.04	0.67	0.104
6	0	0.82	0.15	–	–	1.44	0.63	0.132
7	0	0.82	0.15	106	–	1.71	0.78	0.114
8	0	0.8	0.18	–	–	2.22	1.56	0.179
9	0	0.8	0.18	106	–	2.32	1.65	0.172
10	0	0.82	0.15	–	0.04m 1.36s	2.16	0.86	0.162

(4) and (5)) at orientation angle of 0°, which eventually interconnect to form a narrow channel, leading to a significant increase in scour depth on both sides of the structure and downstream. It is worth noting that, compared to conditions with a lower flow velocity (0.15 m/s), under higher flow velocities (0.18 m/s), the scour process rapidly transitions from a connector-dominated pattern to being influenced by the combination of the connectors and bucket. It leads to the exposure of the bucket from the sand bed. The differences in maximum scour depth resulting from different orientation angles decrease, with a difference of no more than 4 mm between them. Due to the certain dispersion of the scour depths in most scour research and the fact that only three flow velocities were investigated in the present study, it cannot be fully determined whether the scour depth at orientation angle of 0° is consistently greater than that at orientation angle of 30° under high flow velocity conditions.

4.3. Effect of flow pattern on scour characteristics

This study examines three different flow patterns: unidirectional flow, tidal flow, and wave-current interaction. Unidirectional flow is characterized by a constant velocity and consistent flow direction. Tidal flows display periodic fluctuations in both velocity and direction, with maximum velocities reaching 0.15 m/s and 0.18 m/s.

Under unidirectional flow, there is a notable increase in scour intensity, with sediment transport consistently maintaining a single direction. In contrast, under tidal currents, the time of peak velocity within each tidal cycle is relatively short and may occasionally drop below the critical velocity required for sediment movement. During these periods, sediment transport becomes bidirectional, leading to the occurrence of sediment backfilling within the scour hole. Comparative assessments of equilibrium scour topography contours are conducted for Test 1 and 2, 3 and 4, 6 and 7, and 8 and 9. The results indicate that under similar flow velocity conditions, the extent of scour is greater in the x-direction parallel to the current and the y-direction perpendicular to the current under tidal flow. When reaching scour equilibrium, the location of maximum scour depth tends to shift upstream compared to that under unidirectional flow. In Table 3, the scour depth under tidal flow is consistently lower than that under steady unidirectional flow, with the maximum scour depth ranging from 77 to 96 percent of the depth observed in unidirectional flow. Furthermore, the maximum scour depth at higher flow velocities under tidal scour conditions tends to approach that of steady unidirectional flow. Despite the data in Table 3 supporting the conclusions mentioned above, it remains necessary to exercise caution when judging the relationship between scour depths under unidirectional and tidal flows at high velocities. It arises from considerations similar to those in Section 3.1.2 and the potential infill due to the changing direction of tidal flow, which could cause some fluctuations in the equilibrium scour depth.

Only one set of experiments examining the interaction between waves and currents, specifically Test 10, was carried out due to limitations imposed by the test conditions. A comparison of the topography contours of the equilibrium scour between Test 6 and Test 10 (refer to Fig. 19(f)) illustrates that when subjected to wave action in addition to unidirectional flow, the scour around the foundation exhibited increased symmetry. Scour occurred near the connectors (2) and (5), resulting in the rapid downstream formation of scour holes along the flow, extending over a greater distance. The scour depth gradually decreased in the downstream direction, with a sand ridge separating the scour holes on either side, indicating a certain degree of independence without clear interconnections. The maximum length of the scour holes was measured at 216 cm, while the maximum scour depth reached 16.2 cm, surpassing the depth observed in Test 6. Moreover, because of the lower density of the model sand relative to the prototype sand, the sand bed is more susceptible to liquefaction under wave action. It is important to note that the scour depths and scopes might be overestimated.

4.4. Prediction of maximum equilibrium scour depth

The local scour of a mono-column composite bucket foundation (MCCBF) involves complex interactions between water flow, different foundation elements (i.e., mono-column, connectors, and bucket), and the surrounding soil. Factors related to the foundation structure, the sand bed, and hydrodynamic characteristics have varying impacts on scour. These parameters may encompass dimensions of the foundation (D), such as the diameter of the mono-column (D_1) and the bucket diameter (D_2). The median grain size of the sediment (d_{50}) is an optional parameter. Hydrodynamic properties can be characterized by water depth (h), depth-averaged velocity (u), and gravitational acceleration (g). By applying the Buckingham π theorem for quantitative analysis and utilizing various dimensionless parameters, one possible form of the formula describing the equilibrium scour depth (S_{max}) normalized by water depth (h) can be expressed as follows (Guan et al., 2022):

$$\frac{S_{max}}{D} = f\left(Fr, KC, Re, \frac{d_{50}}{D}, \frac{h}{D}\right) \tag{1}$$

Based on a length scale of 1:50, the test data that has been changed to the prototype scale is shown in Table 4. Actually, it is insufficient to support the suggested Eq. (1). In the present study, only a singular sediment type and a specific structural configuration are involved. There is a minimal variation in water depth between different tests (approximately 2% change). Additionally, due to the flow velocity (u) range being from 0.85 m/s to 1.28 m/s, the range of the Froude number (Fr) is extremely narrow (i.e., $0.0424 < Fr < 0.0646$). These parameters are more akin to constants than variables. Only one test related to waves, Test 10, is included in the study, making it inappropriate to use formula that involve the ratio of velocities (U_{cw}) and the Keulegan-Carpenter number (KC) for assessing scour. Therefore, using a very limited amount of experimental data and employing methods such as regression analysis is insufficient to provide a general or even localized empirical expression for predicting the maximum scour depth of a mono-column composite bucket foundation (MCCBF).

Nevertheless, the experimental results were compared with previous studies on predicting scour depth around monopiles under unidirectional flow (Arneson et al., 2012; Briaud, 2004; Sheppard et al., 2014;

Table 4
Foundation scour results at the prototype scale.

NO.	α(°)	h(m)	u (m/s)	T_{tide}(h)	H_m, T_m	L(m)	W(m)	S_{max}(m)	S_{max}/D_1
1	30	40.88	1.05	–	–	42.5	26.5	5.25	0.438
2	30	40.88	1.05	12.4	–	46.5	32	4.05	0.338
3	30	40.08	1.28	–	–	87.5	42	8.8	0.733
4	30	40.08	1.28	12.4	–	122.5	41.5	8.4	0.700
5	0	40.88	0.85	–	–	52	33.5	5.2	0.433
6	0	40.88	1.05	–	–	72	31.5	6.6	0.550
7	0	40.88	1.05	12.4	–	85.5	39	5.7	0.475
8	0	40.08	1.28	–	–	111	78	8.95	0.746
9	0	40.08	1.28	12.4	–	116	82.5	8.6	0.717
10	0	40.88	1.05	–	2m 9.6s	108	43	8.1	0.675

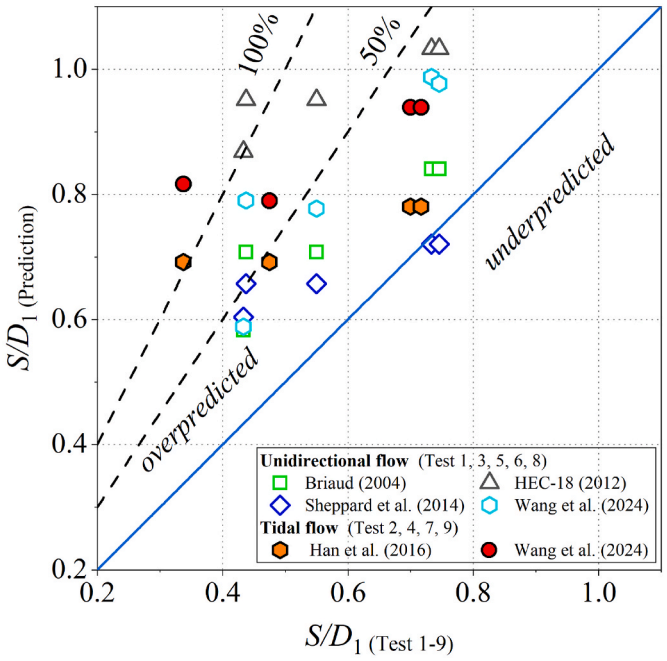

Fig. 20. Comparison of predicted and scour test data.

Wang et al., 2024) and tidal currents (Han et al., 2016; Wang et al., 2024). In the calculations, prototype-scale hydrodynamic conditions, sediment conditions, and structural dimensions were used. The pile diameter was taken as the maximum diameter of the mono-column (D_1 = 12 m). As shown in Fig. 20, almost all predicted values overestimate the scour depth around the MCCBF. Under unidirectional flow, the HEC-18 formula (Arneson et al., 2012) provides the most conservative scour depth estimates. In the scour experiments with lower flow velocities (Test 1 and Test 5), scour depths obtained from the HEC-18 formula up to twice the experimental values were observed (Table 5). The formula proposed by Sheppard et al. (2014) yields the best predictions, especially when the scour depths in the experiments are larger. The percentage difference between the predicted values and the experimental results ranges from −3.7% to +50.3%. For scour under tidal currents, the results from the formula of Han et al. (2016) are closer to the experimental results of this study. For Test 10, the smaller KC number (KC = 0.166) falls outside the applicable range of some prediction formulas (Qi and Gao, 2014; Sumer et al., 1992), making direct application impossible. Therefore, the scour depth data point for Test 10 under combined wave and current action is not shown in Fig. 20. The scour depth observed in Test 10 is 54.1% greater than that in Test 1, which was conducted under unidirectional flow with the same flow velocity (Tables 3 and 4). However, regarding the lack of experimental data, it is important to note the potential overestimation of the impact of waves on scour depth mentioned in Section 3.1.3.

It is important to note that the scour around the MCCBF is mainly influenced by the connectors and the composite bucket. The flow effects around the mono-column are restricted by the shielding of the bucket and the connectors at different orientation angles, preventing them from directly impacting the sand bed. All the aforementioned formulas are intended to predict the local scour depth around monopiles. The significant differences in scour depth caused by varying connector orientation angles at lower flow velocities are not accounted for in these formulas. As a result, almost all methods tend to overestimate the scour depth around the MCCBF, especially when the scour depth of tests is relatively small ($S/D_{1\ (\text{Test 1-9})} < 0.5$, for Test 1, 2, 5, and 7).

In addition to the previous studies on scour depth prediction, there is an alternative method available for the rough estimation of the scour depth of MCCBF. Owing to the unique characteristics of the structure, the streamline contractions and vortices produced by the mono-column are shielded by the composite bucket. The scour process is primarily governed by the connectors and affected by the exposed part of the bucket, leading to a distinctive form of edge scour. Petersen et al. (2015) investigated the edge scour around a monopile with riprap protection. The scour depth can be expressed by the following non-dimensional relationship involving the governing parameters:

$$\frac{S_t}{h_b} = f\left(\theta, \frac{W_b}{D_p}, A_r, \frac{h_b}{D_c}\right) \tag{2}$$

In this formula, S_t represents the equilibrium scour depth at the transverse side of the scour protection, h_b is the berm height of the riprap, θ denotes the Shields number, W_b is the berm width of the riprap, D_p stands for the diameter of the monopile, A_r is the ratio of h_b to W_b, and D_c is the grain size of the riprap. Regarding the prototype MCCBF, S_t in Eq. (2) represents the scour depth at both sides of the bucket; h_b can be interpreted as the portion extending above the sand bed and influencing the scour, and it can be temporarily assumed to be the height of the connectors, which is 12 m. The Shields numbers θ range from 0.428 to 0.970. D_p is considered as the diameter of the mono-column (12 m). W_b

Table 5
Percentage difference in maximum scour depth obtained from various empirical formulas relative to the experimental results.

Test NO.	1	2	3	4	5	6	7	8	9
Briaud (2004)	+61.8%	–	+14.6%	–	+34.5%	+28.7%	–	+12.7%	–
HEC-18	+117.4%	–	+40.8%	–	+100.4%	+72.9%	–	+38.5%	–
Sheppard et al. (2014)	+50.3%	–	−1.7%	–	+39.3%	+19.6%	–	−3.4%	–
Han et al. (2016)	–	+105.0%	–	+11.5%	–	–	+45.7%	–	+8.9%
Wang et al. (2024)	+80.7%	+142.0%	+34.6%	+34.2%	+35.8%	+41.3%	+66.4%	+31.0%	+31.1%

can be taken as the bucket diameter (39 m). Consequently, $W_b/D_p = 3.25$.

Laboratory and field data were used to fit curves showing the relationship between the non-dimensional edge scour depth S_t/h_b and the Shields number for different W_b/D_p ratios (Petersen et al., 2015). It was observed that when W_b/D_p exceeds 3 and θ is greater than 0.1, the normalized equilibrium near-field scour depth at the transverse side of the scour gradually approaches a constant value of 0.85. Consequently, Eq. (2) becomes:

$$\frac{S_t}{h_b} = 0.85 \tag{3}$$

Therefore, S_t is calculated to be 10.2 m. This value exceeds all the scour depths recorded in Table 4, though it is near the highest value of 8.95 m. The results obtained for scour depth using this method hold certain reference values. The differences in scour depth stem from several aspects. Firstly, the roughness and shape of the connector differs from that of the riprap protection and cannot be described by the parameter D_c. Moreover, because of the different arrangements of the connector and riprap, water can pass through the hollow area of the connector. Furthermore, using the height of the connector for h_b may be unreasonable, and its value requires further discussion. With a higher Shields number, Eq. (2) transitions into Eq. (3), leading different flow velocities to produce the same, potentially overly conservative scour depth. The above results suggest that there are numerous challenges in using Eq. (2) to estimate the scour depth of MCCBF. However, it remains a viable method for quickly estimating the maximum scour depth for MCCBFs with dimensions different from those investigated in this study.

5. Summary and conclusions

In this paper, the local scour characteristics around a mono-column composite bucket foundation (MCCBF) are investigated through laboratory experiments. The research investigates the flow dynamics surrounding the MCCBF, analyzing the evolution of scour topography and depth over time. The effects of flow intensities, orientation angles, and different flow patterns on scour development are discussed. The results are summarized as follows.

1. Under the action of unidirectional flow, the scour depth surrounding the connectors experiences rapid development initially. After reaching scour equilibrium, two separate scour holes emerge on either side of the foundation. Typically, there is a lesser scour depth upstream of the foundation, occasionally exhibiting slight siltation. As the flow intensity increases, the scour holes downstream continue expanding along the flow. Concurrently, the scour holes upstream deepen and broaden, possibly resulting in their convergence. The maximum equilibrium scour depth is commonly observed downstream near the connectors.
2. During the initial two tidal cycles, the tidal flow leads to a rapid increase in scour depth around the connectors, with scour holes expanding cyclically both upstream and downstream of the foundation. These holes gradually merge on either side, eventually revealing the bucket buried beneath the sand bed. The scour pattern reaches an equilibrium in an "H" shape along the flow direction. In comparison to scouring under unidirectional flow, tidal flow results in larger-scale scour holes. Typically, the maximum scour depth under tidal flow is found near the upstream connectors of the foundation, except in Test 2. The greater the flow intensities, the closer the maximum scour depth under tidal flow is to the maximum scour depth under unidirectional steady flow.
3. A single experiment was conducted involving the interaction of waves and currents, which led to the creation of a larger scour area with notable scour depth compared to typical unidirectional flow scour patterns. Consideration must be given to the fact that the low-density model sand is more prone to liquefaction under wave action, which can result in an overestimation of the scour depth and extent.
4. At small flow velocities, it was observed that an orientation angle of 0° results in a greater scour depth compared to an orientation angle of 30°, primarily due to the varying effects of connectors on the flow dynamics. Under higher flow velocities, the maximum scour depths at different orientation angles are quite close, making it challenging to ascertain their relative magnitudes. In cases where the orientation angle is set at 0°, the sand bed near the two pairs of connectors can create a narrow overflow channel with the exposed bucket sooner through scouring, leading to distinct differences of scour development between the two orientation angles. Furthermore, there is a streamline contraction around the exposed bucket, which serves to increase flow velocity and enhance the scour around the foundation.
5. Due to the limitations in the amount of experimental data and the range of parameters, no attempt was made to fit a scour depth prediction formula specifically for the MCCBF based on the existing limited data. Instead, the experimental results were compared with the calculation results of other scour depth prediction formulas for monopiles. It was found that almost all the formulas overestimated the scour depth under both unidirectional flow and tidal currents. This discrepancy is attributed to the significant structural differences between monopile foundations and the MCCBF. In some experiments with lower flow velocities, this discrepancy is even more pronounced. The predicted values obtained from empirical formulas can be as much as twice the experimental data. Given that the scour around the MCCBF, primarily influenced by the connector, is similar to edge scour, another approach referenced the estimation strategy for edge scour depth around a monopile with rock protection. Although the parameters and applicability of the formula are subject to further discussion, the results suggest that it remains a viable method for quickly estimating a relatively conservative maximum scour depth and shows potential for application to MCCBFs of different sizes.

CRediT authorship contribution statement

Yuhang Zhang: Writing – original draft, Visualization, Methodology, Investigation, Formal analysis, Conceptualization. **Jinfeng Zhang:** Writing – review & editing, Supervision, Project administration, Conceptualization. **Zhengqi Li:** Writing – review & editing, Investigation, Conceptualization. **Tongqing Chen:** Writing – review & editing, Conceptualization. **Qinghe Zhang:** Writing – review & editing, Conceptualization. **Jiandong Xiao:** Supervision, Resources, Conceptualization.

Declaration of competing interest

The authors declare that they have no known competing financial interests or personal relationships that could have appeared to influence the work reported in this paper.

Data availability

Data will be made available on request.

Acknowledgements

This study was funded by the National Key Research and Development Program of China (Grant No. 2021YFB2601100) and the National Natural Science Foundation of China (Grant No. 51979190). The authors are grateful to Prof. Jerome P.-Y. Maa (the Virginia Institute of Marine Science, College of William & Mary) for his editorial comments on the preparation of figures and texts in this paper.

Appendix A. Scour development for the MCCBFs at smaller velocities

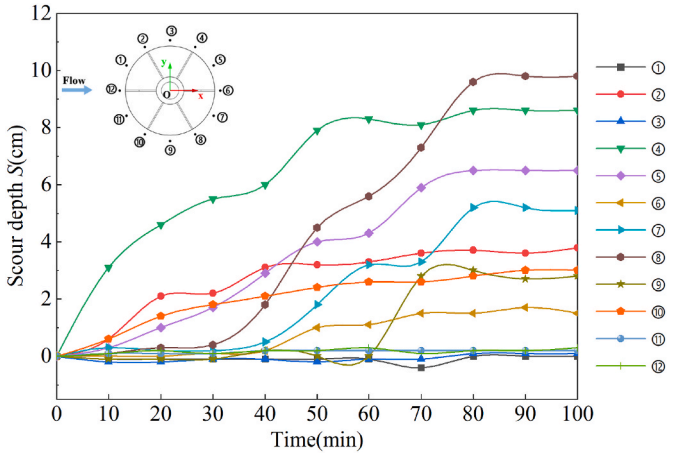

Fig. A.21. Development of scour depth over time at 12 monitoring points of Test 5 ($\alpha = 0°$, $h = 0.82$ m, $u = 0.12$ m/s).

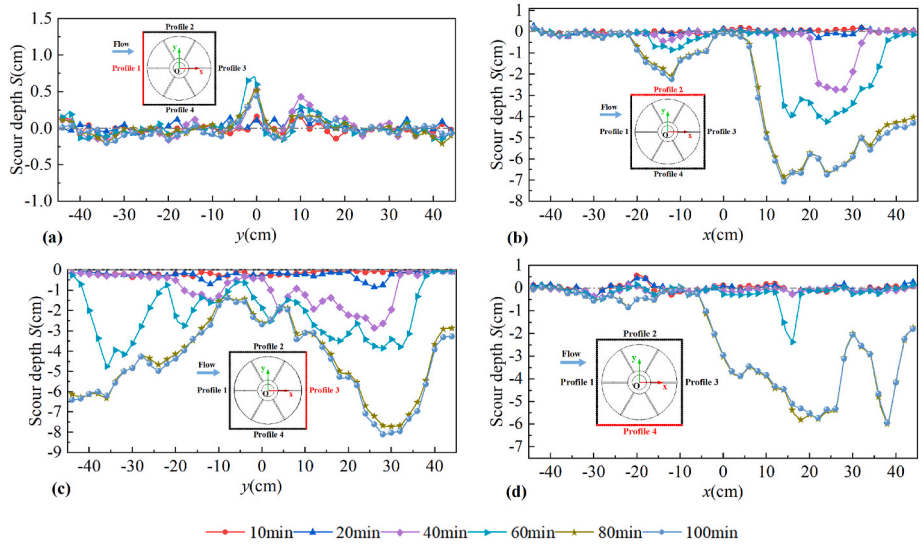

Fig. A.22. Development of scour depth over time in the 4 monitoring profiles of Test5.

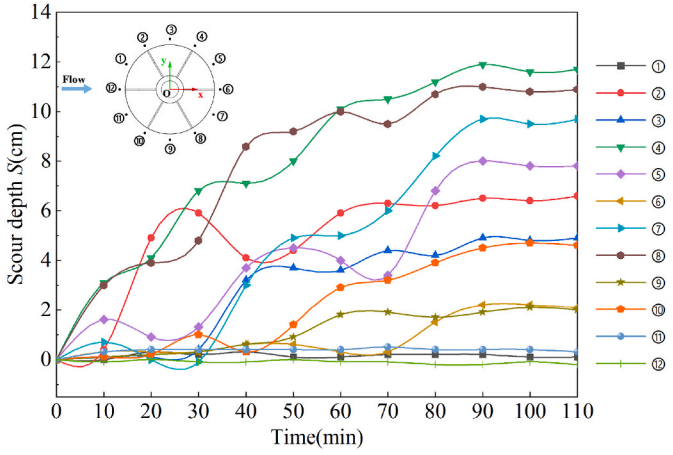

Fig. A.23. Development of scour depth over time at 12 monitoring points of Test 6 ($\alpha = 0°$, $h = 0.82$ m, $u = 0.15$ m/s).

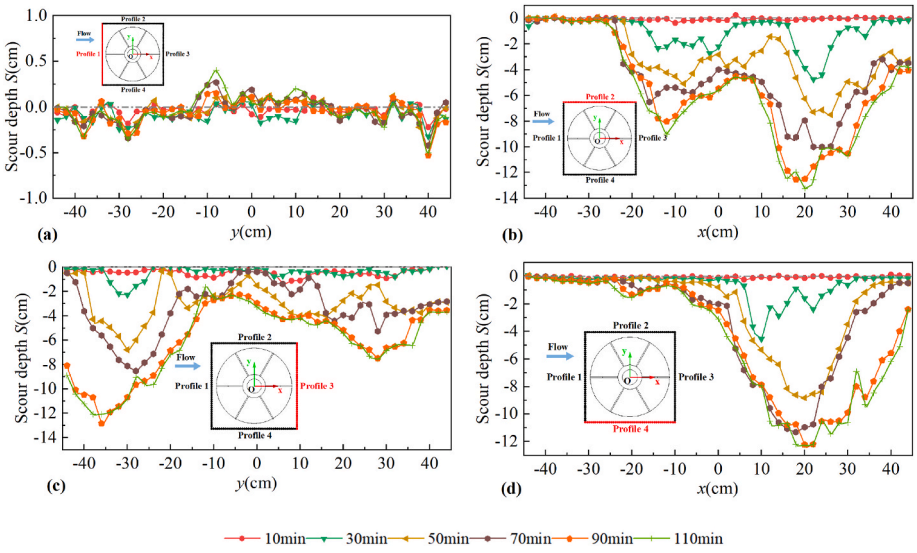

Fig. A.24. Development of scour depth over time in the 4 monitoring profiles of Test6.

Nomenclature

α	Orientation angle (°)
φ	Angle of repose (°)
ρ_s	Sediment density (kg/m^3)
ω	Fall velocity of the sediment particles (mm/s)
θ	Shields number
A_r	The ratio of h_b to W_b,
D_1	Maximum diameter of the mono-column (m)
D_2	Diameter of the composite bucket (m)
D_p	Diameter of the monopile
d_{50}	Median grain size for sediment (mm)
Fr	Froude number
g	Gravitational acceleration (m/s^2)
h	Water depth (m)
h_b	Berm height of the riprap
KC	Keulegan–Carpenter number
L	Maximum length of scour hole parallel to the flow after scour equilibrium (m)
Re	Reynolds number
S	Scour depth (m)
S_{max}	Maximum scour depth (m)
S_t	Equilibrium scour depth at the transverse side of the riprap protection
T_{tide}	Tidal period (h)
U_{cw}	The ratio of velocities for wave and current
u	Mean horizontal velocity along the vertical direction (m/s)
u_c	Critical velocity for sediment (m/s)
W	Maximum width of scour hole vertical to the flow after scour equilibrium (m)
W_b	Berm width of the riprap

References

Arneson, L., Zevenbergen, L., Lagasse, P., Clopper, P., 2012. Evaluating Scour at Bridges. National Highway Institute (US).

Baykal, C., Sumer, B.M., Fuhrman, D.R., Jacobsen, N.G., Fredsøe, J., 2015. Numerical investigation of flow and scour around a vertical circular cylinder. Phil. Trans. Math. Phys. Eng. Sci. 373 (2033), 20140104.

Briaud, J.L., 2004. Pier and Contraction Scour in Cohesive Soils, vol. 516. Transportation Research Board.

Chen, B., Li, S., 2018. Experimental study of local scour around a vertical cylinder under wave-only and combined wave-current conditions in a large-scale flume. J. Hydraul. Eng. 144 (9), 04018058.

Chen, S., Gong, E., Zhao, X., Arikawa, T., Chen, X., 2022. Large-scale experimental study on scour around offshore wind monopiles under irregular waves. Water Sci. Eng. 15 (1), 40–46.

Cheng, H., Cheng, Y., Wang, X., Xia, B., Lyu, X., Zheng, Y., Zhang, J., 2022. Experimental study of local scour around inclined piles in combined waves and current. Ocean Eng. 266, 112511.

Dey, S., Sumer, B.M., Fredsøe, J., 2006. Control of scour at vertical circular piles under waves and current. J. Hydraul. Eng. 132 (3), 270–279.

Esteban, M., López-Gutiérrez, J.-S., Negro, V., 2019. Gravity-based foundations in the offshore wind sector. J. Mar. Sci. Eng. 7 (3), 64.

Guan, D., Chiew, Y.M., Melville, B.W., Zheng, J., 2019. Current-induced scour at monopile foundations subjected to lateral vibrations. Coast. Eng. 144, 15–21.

Guan, D., Xie, Y., Yao, Z., Chiew, Y., Zhang, J., Zheng, J., 2022. Local scour at offshore windfarm monopile foundations: a review. Water Sci. Eng. 15 (1), 29–39.

Han, H., Xiong, S., Sun, Z., 2016. Local scour equation at bridge piers under tidal current action. J. Sediment. Res. (1), 9–13.

Ji, C., Zhang, J., Zhang, Q., Li, M., Chen, T., 2018. Experimental investigation of local scour around a new pile-group foundation for offshore wind turbines in bi-directional current. China Ocean Eng. 32, 737–745.

Li, Z., Hu, P., Ma, J., Gao, M., Huang, H., Liu, X., Qi, L., Sun, Z., 2022. Analysis and prospect of offshore wind power development in China. China Offshore Oil Gas 34 (5), 229–236.

Lian, J., Li, J., Guo, Y., Wang, H., Yang, X., 2022. Numerical study on local scour characteristics of multi-bucket jacket foundation considering exposed height. Appl. Ocean Res. 121, 103092.

Liang, D., Jia, H., Xiao, Y., Yuan, S., 2022. Experimental investigation of turbulent flows around high-rise structure foundations and implications on scour. Water Sci. Eng. 15 (1), 47–56.
Ma, H., Yang, J., Chen, L., 2018. Effect of scour on the structural response of an offshore wind turbine supported on tripod foundation. Appl. Ocean Res. 73, 179–189.
Oh, K.Y., Nam, W., Ryu, M.S., Kim, J.Y., Epureanu, B.I., 2018. A review of foundations of offshore wind energy convertors: current status and future perspectives. Renewable Sustainable Energy Rev. 88, 16–36.
Petersen, T.U., Sumer, B.M., Fredsøe, J., Raaijmakers, T.C., Schouten, J.-J., 2015. Edge scour at scour protections around piles in the marine environment—laboratory and field investigation. Coast. Eng. 106, 42–72.
Qi, W., Gao, F., 2014. Equilibrium scour depth at offshore monopile foundation in combined waves and current. Sci. China Technol. Sci. 57, 1030–1039.
Roulund, A., Sumer, B.M., Fredsøe, J., Michelsen, J., 2005. Numerical and experimental investigation of flow and scour around a circular pile. J. Fluid Mech. 534, 351–401.
Rudolph, D., Bos, K.J., 2006. Scour around a monopile under combined wave-current conditions and low kc-numbers. Proceedings of the Sixth International Conference on Scour and Erosion, pp. 582–588.
Saud Afzal, M., Bihs, H., Kamath, A., Arntsen, Ø.A., 2015. Three-dimensional numerical modeling of pier scour under current and waves using level-set method. J. Offshore Mech. Arctic Eng. 137 (3), 032001.
Sheppard, D., Melville, B., Demir, H., 2014. Evaluation of existing equations for local scour at bridge piers. J. Hydraul. Eng. 140 (1), 14–23.
Sogut, E., Hsu, T.-J., Farhadzadeh, A., 2022. Experimental and numerical investigations of solitary wave-induced non-equilibrium scour around structure of square cross-section on sandy berm. Coast. Eng. 173, 104091.
Song, Y., Xu, Y., Ismail, H., Liu, X., 2022. Scour modeling based on immersed boundary method: a pathway to practical use of three-dimensional scour models. Coast. Eng. 171, 104037.
Stahlmann, A., Schlurmann, T., 2010. Physical modeling of scour around tripod foundation structures for offshore wind energy converters. In: Proceedings of the Coastal Engineering Conference, 2010.
Sumer, B.M., 2002. The mechanics of scour in the marine environment. World Scientific, 981-02-4930-6.
Sumer, B.M., Fredsøe, J., Christiansen, N., 1992. Scour around vertical pile in waves. J. Waterw. Port, Coast. Ocean Eng. 118 (1), 15–31.
Tao, J., Chen, Y., Huang, B., 2023. Current situation and development trend of offshore wind power. Energy Eng. J. Assoc. Energy Eng. 43 (4), 1–9.
Wang, S., Qi, W., Li, B., Wang, C., Gao, F., 2024. Tidal currents-induced scour development around pile foundations: effects of flow velocity hydrograph. Coast. Eng. 191, 104533.
Wang, Y.-H., Jiang, W.-G., Wang, Y.-H., 2021. Scale effects in scour physical-model tests: cause and alleviation. J. Mar. Sci. Technol. 21 (5), 5.
Wu, X., Hu, Y., Li, Y., Yang, J., Duan, L., Wang, T., Adcock, T., Jiang, Z., Gao, Z., Lin, Z., Borthwick, A., Liao, S., 2019. Foundations of offshore wind turbines: a review. Renewable Sustainable Energy Rev. 104, 379–393.
Xiao, J., Zhang, Q., Lin, Y., Wang, L., Chen, L., Ca, X., 2020. A connection tool for combined foundation of mono column and composite bucket. China, Patent CN210737581U, issued June 12.
Yang, Q., Yu, P., Liu, Y., Liu, H., Zhang, P., Wang, Q., 2020. Scour characteristics of an offshore umbrella suction anchor foundation under the combined actions of waves and currents. Ocean Eng. 202, 106701.
Yu, T., Lian, J., Shi, Z., Wang, H., 2016. Experimental investigation of current-induced local scour around composite bucket foundation in silty sand. Ocean Eng. 117, 311–320.
Yu, T., Zhang, Y., Zhang, S., Shi, Z., Chen, X., Xu, Y., Tang, Y., 2019. Experimental study on scour around a composite bucket foundation due to waves and current. Ocean Eng. 189, 106302.
Yuan, C., Melville, B.W., Adams, K.N., 2017. Scour at wind turbine tripod foundation under steady flow. Ocean Eng. 141, 277–282.
Zhang, H., Liang, F., Zheng, H., 2021. Dynamic impedance of monopiles for offshore wind turbines considering scour-hole dimensions. Appl. Ocean Res. 107, 102493.
Zhang, P., Qi, X., Ding, H., Le, C., Lin, Y., Xiao, J., 2023. Bearing characteristics of mono-column composite bucket foundation in sand for offshore wind turbines. Ocean Eng. 280, 114870.
Zhang, W., Uh Zapata, M., Bai, X., Pham-Van-Bang, D., Nguyen, K.D., 2020. Three-dimensional simulation of horseshoe vortex and local scour around a vertical cylinder using an unstructured finite-volume technique. Int. J. Sediment Res. 35 (3), 295–306.
Zhao, M., Cheng, L., Zang, Z., 2010. Experimental and numerical investigation of local scour around a submerged vertical circular cylinder in steady currents. Coast. Eng. 57 (8), 709–721.